Critical analysis of the Holocene palaeointensity database in Central America: Impact on geomagnetic modelling

Gwenaël Hervé, Mireille M. Perrin, Luis Alva-Valdivia, Brina Madingou Tchibinda, Alejandro Rodriguez-Trejo, Arnaldo Hernandez-Cardona, Mario Córdova Tello, Carolina Meza Rodriguez

Critical analysis of the Holocene palaeointensity database in Central America: impact on geomagnetic modelling

Gwenaël Hervé[1], Mireille Perrin[1], Luis Alva-Valdivia[2], Brina Madingou Tchibinda[1], Alejandro Rodriguez-Trejo[2], Arnaldo Hernandez-Cardona[2], Mario Córdova Tello[3], Carolina Meza Rodriguez[3]

[1] Aix Marseille Univ, CNRS, IRD, INRA, Coll France, CEREGE, Aix-en-Provence, France

[2] Universidad Nacional Autónoma de México: Instituto de Geofísica, Laboratorio de Paleomagnetismo, Mexico City, Mexico.

[3] Instituto Nacional de Antropologia e Historia, Centro Morelos, Mexico.

Abstract

Thanks to its rich archaeological heritage, Central America is a key region to recover the past secular variation of the geomagnetic field. This article presents 13 new palaeointensity data on Epiclassic (650 – 900 CE) pottery sherds from Central Mexico. Archaeointensities were determined using the Thellier-Thellier protocol with anisotropy and cooling rate corrections. Average results between 25 and 42 μT reveals a fast secular variation in the second half of the first millennium CE but are not in agreement with global geomagnetic models that predict a higher geomagnetic field strength. To check the reasons of this discrepancy, we compiled all intensity data over the last millennia published in Central America. The Bayesian curve calculated from 194 data covering the last 4 millennia highlights a rapid succession of oscillations of the geomagnetic field strength between 20 and 80 μT. But a critical analysis of the dataset shows a large influence of data quality, 74% of them having a poor cooling unit consistency and experimental quality. The small number of specimens per cooling unit and the anisotropy correction absent or incorrectly made increase the scatter between data, whereas the absence of cooling rate correction biases the dataset towards higher palaeointensity. Discarding these data results in a lower secular variation by removing most extreme values and several intensity oscillations. The weaknesses of the dataset are likely the main reason of the limitations of global models in Central America. Pending the acquisition of new high-quality data, archaeomagnetic dating seems premature in Central America.

Keywords

Geomagnetic secular variation; Palaeointensity; Central America; Ceramics

1. Introduction

Ground-based and satellite measurements of the geomagnetic field, together with numerical models of the geodynamo, provide a priceless insight of the flux dynamic in the Earth's core. However, this knowledge is limited in time because direct absolute measurements cover a short era, at the most the last four centuries. Beyond, secular variation is recovered from archaeological baked clays, volcanic lava flows and marine or lacustrine sediments. The first two materials acquire a thermoremanent magnetization (TRM) during their last high-temperature heating and give an absolute but discrete estimation of the direction and intensity of the past geomagnetic field. Sediments have the advantage to provide a continuous record of the secular variation but palaeointensity and declination are only relative and require a calibration with absolute data (Panovska et al., 2015).

Several global models of the Holocene secular variation have been developed by inversion of data using spherical harmonic analysis in space (e.g. Constable et al., 2016; Hellio & Gillet, 2018; Licht et al., 2013; Nilsson et al., 2014; Pavón-Carrasco et al., 2014a). These models are powerful tools to investigate the evolution of the geomagnetic patterns at the core-mantle boundary (e.g. Constable et al., 2016) and to scale cosmogenic nuclides production (Lifton, 2016). The local predictions of the global models are also more and more used for archaeomagnetic dating purposes (e.g. Goguitchaichvili et al., 2016). However, these global models tend to smooth the amplitude of the secular variation observed in regional master curves (e.g. Tema et al., 2017 in Hawaii; Cai et al., 2016 in China; Hervé et al., 2017 in Western Europe), especially for the intensity variations and even more when models include relative sedimentary data. Models built only with absolute data would better fit the data but their spatial and temporal distribution is very uneven, with ~70% of them coming from West Eurasia and North Africa and ~70% dated in the last two millennia. Data are especially lacking in the south hemisphere.

Another limitation is the unequal quality of the data. The impact of this factor on geomagnetic modelling is often underestimated, although it has been demonstrated with the European model SCHA.DIF.3k (Pavón-Carrasco et al., 2014b). The archaeomagnetic databases, the most complete one being Geomagia50 (Brown et al., 2015), compile all results without *a priori* assessment on the quality of the data point. However, the quality is clearly heterogeneous, as depicted by the number of samples, the experimental and temporal uncertainties and the laboratory protocols. Here, we first present thirteen new intensity data acquired on potteries from Chalcatzingo in Mexico, before to show the influence of a critical analysis on the knowledge of secular variation of the geomagnetic field with the example of the intensity in Central America.

2. New archaeointensity data

2.1 Archaeological context and sampling

Chalcatzingo (Lat: 18.6766°N, Long: 98.7705°W) is located in the Amatzinac valley (Morelos state) at circa 120 km South-East of Mexico City (Figure 1). The archaeological site has been excavated since the 30s and presently Mario Córdova Tello and Carolina Meza Rodriguez from the *Instituto Nacional de Antropologia e Historia* (INAH) direct the research program. The site was mainly occupied between 800 and 500 BCE during the Preclassic period. The archaeological remains, the most famous being the Olmec style petroglyphs, attest of the importance of the site in the region (e.g. Grove, 1987). The occupation continued later in the Classic (200-650 CE), Epiclassic (650-900 CE) and Postclassic (900-1500 CE) periods of the Central Mexico chronology.

This study focused on the Epiclassic layers from the Terrace 6 "*El Cazador*", close to the main square and the pyramid. We sampled 16 sherds of six pottery-types, characteristic of

this period in the Amatzinac valley (Martin Arana, 1987): *negro pulido* (2 sherds), *anaranjado rojo estriado* (3), *anaranjado pulido* (2), *anaranjado burdo* (3), *estriado sin engobe* (3) and *Coyotlatelco* (3).

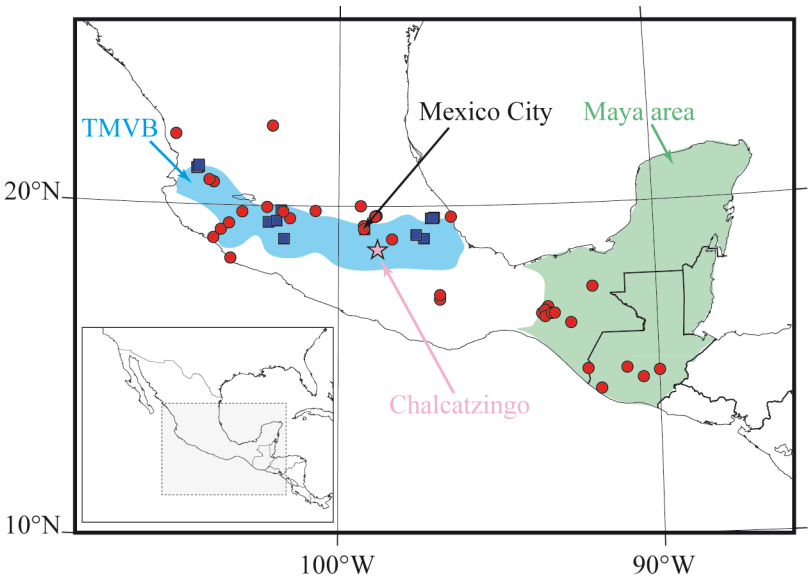

Figure 1: Spatial distribution of Central America data over the last 4 kyrs. Archaeomagnetic (volcanic) data are plotted in red (blue). The pink star indicates the location of Chalcatzingo. TMVB is the abbreviation of Trans Mexican Volcanic Belt

2.2 Rock magnetism

Thermomagnetic curves were measured on powders from six sherds using Agico MFK1 apparatus. The variation of the susceptibility was measured during heating to 450 °C or 620 °C and subsequent cooling. All thermomagnetic curves were reversible, highlighting the suitability of Chalcatzingo sherds for archaeointensity experiments. We observed two groups of specimens. The types *anaranjado rojo estriado*, *anaranjado pulido* and *negro pulido* showed a single ferromagnetic carrier, identified as a Ti-poor titanomagnetite by the Curie temperature around 550 °C (Figure 2a). The *Coyotlatelco*, *estriado sin engobe* and

105 *anaranjado burdo* types presented a second phase with a Curie temperature close to 150 °C
106 (Figure 2b), which can be a Ti-rich titanomagnetite or an epsilon iron oxide (ε-Fe_2O_3) (Lopez-
107 Sanchez et al., 2017).

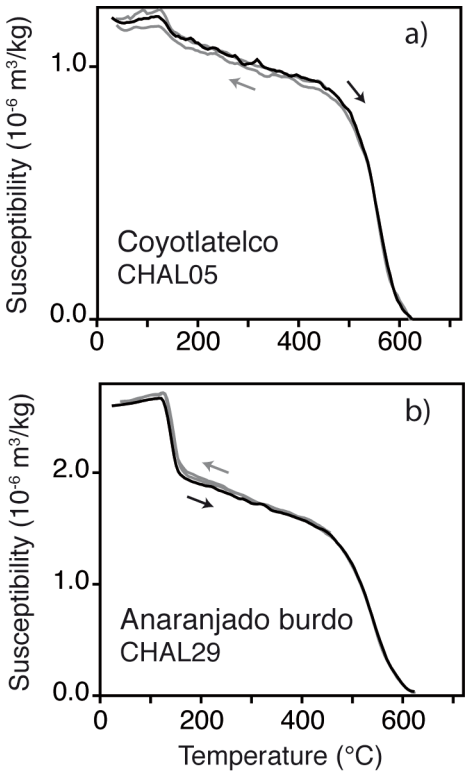

108

109 Figure 2: Representative thermomagnetic curves of Epiclassic sherds from Chalcatzingo.

110

111 2.3 Archaeointensity study

112 Archaeointensity experiments were conducted on 0.6 to 3.0 g specimens embedded in 2 cm
113 cubes of amagnetic plaster. We used the classical Thellier-Thellier method (Thellier &
114 Thellier, 1959) that consists to heat and cool twice the specimens at each temperature step
115 with a laboratory field applied in both directions of a specimen axis (+z, -z). We performed
116 partial thermoremanent magnetization (pTRM) checks every two steps to monitor the absence
117 of alteration of the ferromagnetic mineralogy. Heating was performed in an ASC TD-48SC
118 furnace with a 30 or 40 μT laboratory field using 9-12 temperature steps up to 620 °C. In total

we studied 3 to 5 specimens per sherd for a total of 54 specimens. Measurements were realized on a SQUID cryogenic magnetometer (2G Enterprises, model 755R) at CEREGE.

The archaeointensities were corrected for the effects of TRM anisotropy and cooling rate. The TRM anisotropy tensor was determined at 550 °C using 6 positions (+x, -x, +y, -y, + z and –z axes) followed by a stability check (Chauvin et al., 2000). The cooling rate procedure of Gómez-Paccard et al. (2006) was carried out at the same temperature with a slow cooling over 5 h. This duration, explained by experimental constraints, may underestimate the archaeological cooling but an incorrect estimation of the duration seems to have a low impact on the accuracy of the archaeointensity (Hervé et al., accepted). The anisotropy and cooling rate corrections were applied at the specimen level.

Almost all specimens presented a secondary component of magnetization. The characteristic remanent magnetization (ChRM) was isolated above 150-500 °C. The secondary component could be acquired during the cooking use of the pot or since the excavations in the archaeological repository. Except for one sherd, the fraction of the NRM in the ChRM (f factor) was higher than our acceptance value equal to 0.35. Forty-five specimens presented a linear NRM-TRM diagram with positive pTRM-checks on the temperature interval of the ChRM (Figure 3a-c). The nine other specimens were rejected because of mineralogical changes, as indicated by non-linear NRM-TRM diagram and negative pTRM-checks (Figure 3d). No results could be obtained for the two sherds of the type *negro pulido* and for one of the type *estriado sin engobe*. Accepted specimens fulfil up-to-date quality criteria with a quality factor (q) between 5 and 80 (Table 1S, Supplementary Material). Almost all specimens had a ratio of the standard error of the slope to the absolute value of the slope (ß) lower than 0.05, a deviation angle (DANG) lower than 5° and a maximum angular deviation (MAD) lower than 5°.

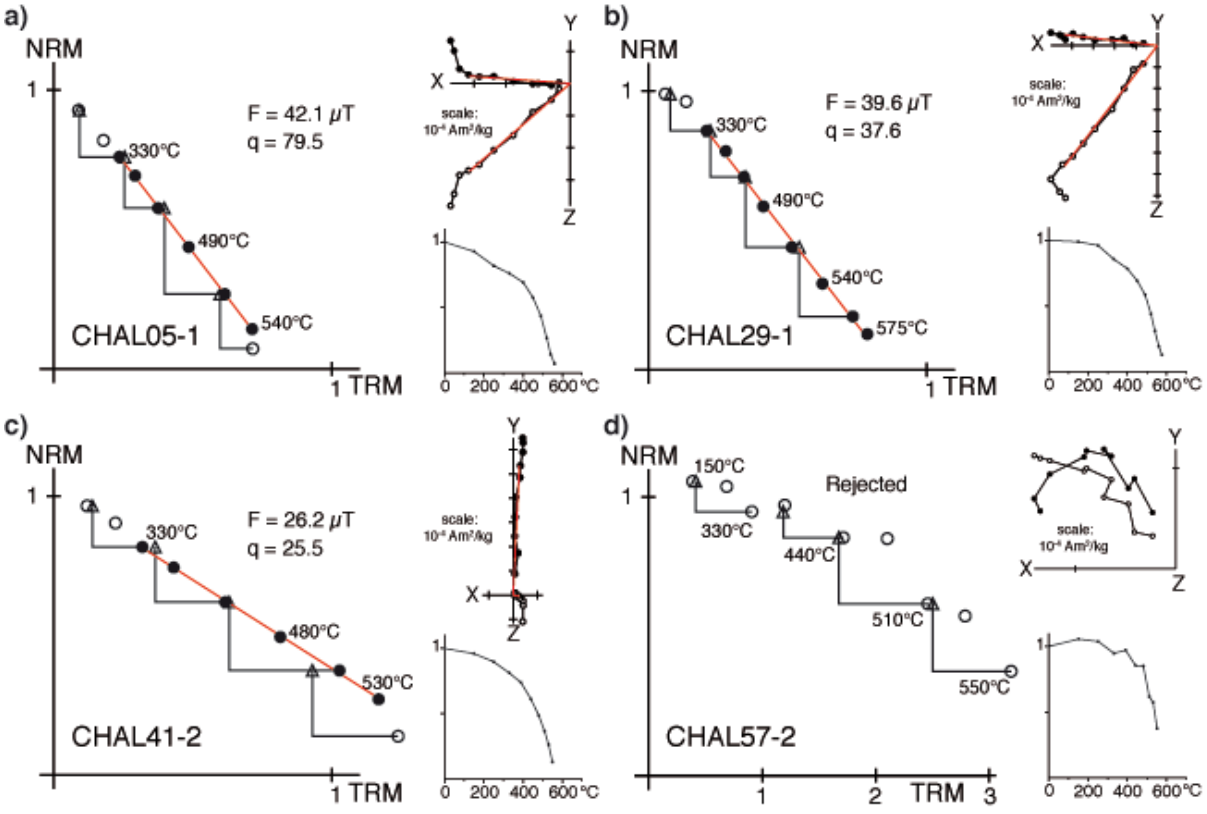

Figure 3: Representative accepted (a-c) and rejected (d) archaeointensity results with NRM-TRM diagrams, orthogonal plots and demagnetization curves.

Table 1 listed the 13 new average archaeointensities. All were calculated with three or four specimens and have an experimental uncertainty between 1.5 and 9.5%. The range of the average values between 25 and 42 µT tend to indicate a fast secular variation during the second half of the first millennium CE. No clear relationship is observed between the archaeointensity and the pottery-type. On Figure 4a, data are relocated to Mexico City using the Virtual Axial Dipole Moment (VADM) correction and compared to the regional curve of Goguitchaichvili et al. (2018a). The curve was computed using a bootstrap approach from 67 data from Mesoamerica and 17 from southwest United States. Our data matches the curve, except CHAL23 and CHAL41 that are below the curve.

Type of pottery	Sherd	N_{acc}/N_{meas}	$F_{ATRM+CR}$ ± SD (μT)	$F_{Mexico\ City}$ (μT)	VADM (10^{22} A.m^2)
Anaranjado rojo estriado	CHAL01	4/5	35.1 ± 3.0	35.4	7.9 ± 0.7
	CHAL02	3/5	34.5 ± 2.6	34.8	7.8 ± 0.6
	CHAL03	4/5	34.9 ± 1.0	35.2	7.9 ± 0.2
Coyotlatelco	CHAL04	3/4	31.5 ± 3.0	31.8	7.1 ± 0.7
	CHAL05	4/4	39.5 ± 2.0	39.9	8.9 ± 0.5
	CHAL06	3/4	42.3 ± 0.7	42.7	9.6 ± 0.2
Estriado sin engobe	CHAL22	4/4	36.4 ± 2.9	36.7	8.2 ± 0.7
	CHAL23	3/3	28.3 ± 0.9	28.6	6.4 ± 0.2
Anaranjado burdo	CHAL29	4/4	37.8 ± 0.7	38.1	8.5 ± 0.2
	CHAL30	3/3	39.7 ± 2.4	40.1	9.0 ± 0.5
	CHAL31	4/4	36.9 ± 1.8	37.2	8.3 ± 0.4
Anaranjado pulido	CHAL40	3/3	41.1 ± 2.0	41.5	9.3 ± 0.5
	CHAL41	3/3	24.7 ± 1.4	24.9	5.6 ± 0.3

157 Table 1: Average archaeointensities of Epiclassic sherds from Chalcatzingo. Columns from
158 left to right: type of potteries, name of the sherd, number of accepted over measured
159 specimens, average archaeointensity corrected for the effects of TRM anisotropy and cooling
160 rate with its standard deviation, average archaeointensity relocated to Mexico City, Virtual
161 Axial Dipole Moment.

162

Global models CALS10k.2 (Constable et al., 2016), SHA.DIF.14k (Pavón-Carrasco et al., 2014a) and COV-ARCH/COV-LAKE (Hellio & Gillet, 2018) give consistent predictions at Mexico City. SHA.DIF.14k and COV-ARCH were calculated using archaeomagnetic and volcanic data, whereas CALS10k.2 and COV-LAKE also include lacustrine and marine sedimentary data. Models also differ by the inverse method. CALS10k.2 and SHA.DIF.14k imposed regularizations in space and time. The stochastic approach of COV-ARCH and COV-LAKE used the temporal statistics from satellites, ground-based and palaeomagnetic data as prior information through cross-covariance functions. The four models fit only the highest Chalcatzingo values. Their predictions are usually above the regional master curve of Goguitchaichvili et al. (2018a) and predict a slower secular variation.

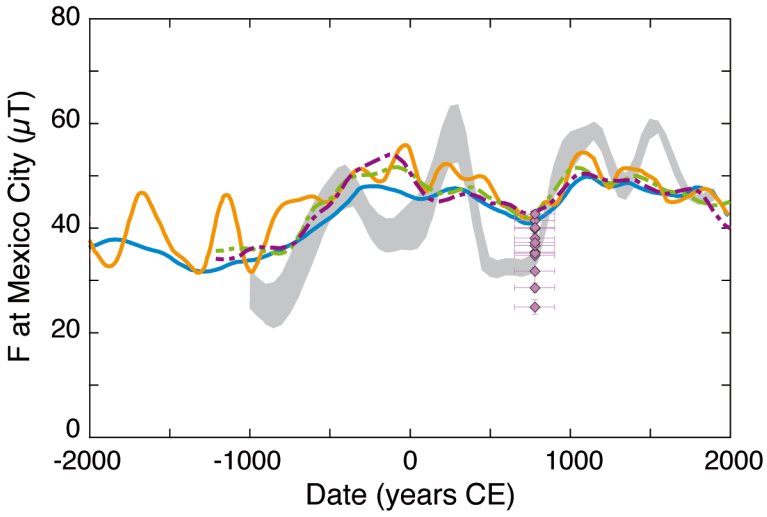

Figure 4: Comparison of Chalcatzingo data relocated to Mexico City (in pink) with the bootstrap regional curve of Goguitchaichvili et al. (2018a) (in grey) and with the predictions of global models CALS10k.2 (Constable et al. 2016, blue curve), SHA.DIF.14k (Pavon-Carrasco et al, 2014a, orange curve), COV-ARCH and COV-LAKE (Hellio & Gillet, 2018, green and purple dotted curves).

3. Compilation of Central America intensity data

In order to check the reason of these discrepancies, we compiled all intensity data from Central America from the original articles (Figure 5a). We carried out the critical analysis only on the last four millennia because data are much too scarce before (5 data between 5000 and 2000 BCE).

A data point is defined as a cooling unit that acquired TRM at the same time, such as a volcanic lava flow, an archaeological kiln or fireplace and a single pottery. For ceramics, a data point is sometimes defined in the literature as the average of independent pots (e.g. Genevey et al., 2016; Gómez-Paccard et al., 2016; Hervé et al., 2017), because they were discovered in a single homogeneous short-lived archaeological feature. This is not the case in Chalcatzingo and in most studies. Even if ceramics were dated in the same period, the probability of no contemporaneous cooling is high, because sherds came from different archaeological layers or from a single layer associated to a long-lived settlement.

The total number of intensity data in Central America over the last four millennia is 194 (including the 13 new data from Chalcatzingo) out of 40 different papers (Tab. 2S in Supplementary Material). 86% of these studies have been published after the 2000s. Data from 16 studies are not yet included in the Geomagia database (this study; Böhnel et al., 2016; Cifuentes-Nava et al., 2017; Goguitchaichvili et al., 2017, 2018b, 2018c; Herrero-Bervera, 2015; Lopez-Tellez et al., 2008; Mahgoub et al., 2017a, 2017b; Michalk et al., 2010; Morales et al., 2012, 2013, 2015; Rodriguez-Ceja et al., 2012; Terán et al., 2016). With this update, our dataset is almost twice larger than the one used in a recently published compilation of Mesoamerica (Goguitchaichvili et al., 2018a) that contains 106 data with only one study (Böhnel et al., 2016) published in the last five years.

Data are concentrated in Central Mexico around the 20°N parallel and in the Mayan area (Chiapas-Guatemala) (Figure 1). Archaeological baked artefacts (here bricks, burnt walls,

206 burnt soils and ceramics) constitute 87% of the dataset (168 data), the rest coming from
207 volcanic lava flows of the Trans Mexican Volcanic Belt (TMVB). Only 17 data (9%), all
208 volcanic, are full vector data.

209 Fifty-four cooling units were dated by radiocarbon. When the uncalibrated age was provided,
210 we updated the date of the archaeomagnetic site using the most recent calibration curve
211 IntCal13 (Reimer et al., 2013). In the case of Xitle lava flow, we used the newest age,
212 1670±35 uncal. BP, of Siebe (2000). Twelve data come from historical eruptions since the
213 Spaniards conquest, the youngest being the Paricutin in 1943-1952. For the 115 others data
214 (i.e. 58%), the dating was defined by stratigraphy or typology of archaeological artefacts. The
215 temporal density of data is higher in the periods of Late Preclassic (circa 400 BCE – 200 CE),
216 Classic (circa 200 – 650 CE) and the youngest half of Postclassic (circa 1200 – 1500 CE)
217 (Figure 5a). Two important gaps are observed, the first between 800 and 400 BCE and the
218 youngest around 1000 CE.

219 The intensity values over the last 4 kyrs range between ~15 μT and ~90 μT (Figure 5b). The
220 dataset looks cloudy, especially in the third and four centuries CE with values from 15 μT up
221 to 75 μT. The spread is visually increased by the fact that many data are dated in the same age
222 interval corresponding to an archaeological period, generally wide of several centuries. This
223 tends to divide the dataset in successive time slices, modelled on the archaeological
224 chronologies. The variability of intensities may reflect the secular variation within each
225 archaeological period.

226 An intensity secular variation curve was computed using a Bayesian framework (Hervé et
227 Lanos, 2018; Lanos, 2004; Schnepp et al., 2015). The curve is given as a smooth continuous
228 curve obtained by averaging cubic splines and took into account experimental and age
229 uncertainties as prior information. The misfit of each data to the curve is minimised by
230 exploring the multidimensional space of probability densities using Monte Carlo Markov

231 Chains. The curve presents a rapid succession of oscillations of the geomagnetic field
232 strength, especially from 400 BCE to 1500 CE, at the time of the highest data density. The
233 oscillations represent the best fit to the intensity variability within the time slices related to
234 age uncertainties. They can imply a fast secular variation of many dozens of μT over a few
235 centuries, similar to the rates observed in the Levantine area at the beginning of the first
236 millennium BCE (Shaar et al., 2011). But it can also reflect experimental problems and a
237 critical analysis of the database has to be performed, before to evoke a geomagnetic
238 phenomenon.

239

240 **4. Critical analysis**

241 4.1 Challenges in palaeointensity determination

242 The linearity between the intensity of the thermoremanent magnetization and the past
243 geomagnetic field strength is the physical basis of the palaeointensity determination.
244 Acquiring reliable data remains a challenging task because several effects can lead to a
245 departure away from the linearity (see Dunlop 2011 for a review). The required reciprocity of
246 blocking and unblocking temperatures is only verified for single-domain grains without
247 interactions. Alteration of the magnetic grains when heated at the laboratory is another cause
248 of failed experiments. Moreover, palaeointensities should be determined only on the
249 Characteristic Remanent Magnetization (ChRM) acquired during the last heating above the
250 Curie point. A calculation including a secondary component of magnetization can differ by a
251 few dozens of μT from the intensity calculated on the sole ChRM (Hervé et al., 2013).

252 The Thellier-Thellier protocol (Thellier & Thellier, 1959) and its derived versions are
253 admitted as the most reliable to control the respect of these conditions thanks to the

progressive heating steps and the use of pTRM-checks. But the multiple heatings increase the risk of alteration and alternative protocols were developed.

The microwave (MW) technique (Walton, 1991; Walton & Böhnel, 2008) is based on microwave absorption by magnetic grains using progressive frequency steps, which reduces the heating temperature of the sample. This method does not exactly replicate the acquisition process of the initial TRM, as ferromagnetic grains are excited by magnons instead of phonons in the usual thermal techniques.

The multispecimen (MSP) method is performed on a set of specimens from the same sample. All specimens are heated once at the same temperature (usually in the 300-400 °C temperature range) in different laboratory field values applied parallel to the NRM (Dekkers & Böhnel, 2006). The comparison of the demagnetized NRM intensity with the one of the acquired partial-TRM provides the palaeointensity. The Central American MSP data were obtained with the original protocol of Dekkers & Böhnel (2006), which do not correct for the NRM fraction and domain state as advised by Fabian & Leonhardt (2010). They are therefore likely overestimated (Schnepp et al., 2016).

Finally, the Shaw method (Shaw, 1974) compares the alternating field (AF) demagnetization of the NRM with the one of a full laboratory TRM. The scaling factor between the two demagnetizing curves is an estimate of the ratio between ancient and laboratory fields. But the linearity between the magnetization and geomagnetic field cannot be checked and the palaeomagnetic community generally considers this method of lower quality.

It is well known that the cooling rate has an important effect on the palaeointensity of archaeological baked clays. The TRM intensity of single-domain grains increases with the cooling rate duration (e.g. Dodson and McClelland-Brown, 1980). As the laboratory cooling is faster than the archaeological cooling, uncorrected palaeointensities are generally overestimated. In the case of the volcanic lava flows, the correction is usually not considered

279 necessary, because the coarser mineralogy makes them less sensitive to the cooling rate
280 effect. For the thick Xitle lava flow, the correction improves the precision of the
281 palaeointensity but does not change significantly the palaeointensity average (Morales et al.,
282 2006) (Table 4S).

283 The anisotropy correction is also crucial depending on the type of material. The preferential
284 alignment of the iron oxides during the manufacturing process of baked clays results in
285 distortion of the NRM with respect to the surrounding geomagnetic field (Veitch et al., 1984).
286 Potteries are generally anisotropic and palaeointensity can sometimes be biased up to a factor
287 of two (e.g. Hervé et al., 2017; Osete et al., 2016). The effects can also be high in burnt walls
288 and soils (Palencia-Ortas et al., 2017; Molina-Cardin et al., 2018). Conversely, the influence
289 of the TRM anisotropy is assumed negligible in lava flows. But the robustness of this
290 presupposition can be questioned, as the anisotropy of magnetic susceptibility (AMS) is often
291 significant and used as a proxy for flow direction (e.g. Fanjat et al., 2012).

292 Two different anisotropy corrections were used in the Central American dataset, first the
293 determination of the TRM tensor at the specimen level (Chauvin et al., 2000, see section 2.3)
294 and secondly a method, peculiar to Mexico, that we called in the following Mean(XYZ)
295 method. Each baked clay fragment is cut in 6 mini-specimens keeping the same orientation.
296 The laboratory field during the Thellier experiments is applied along +x axis for one
297 specimen, -x for another one and +y, -y, +z or –z axis for the four others. Averaging of the six
298 individual intensity estimations is considered to properly correct the TRM anisotropy effect.
299 Poletti et al. (2016) questioned the reliability of this approach. They calculated the TRM
300 tensor at two different temperatures and then roughly determined the intensities from the
301 slope between the two +x TRMs (and -x…) on the NRM-TRM diagram. Their results show
302 that the Mean(XYZ) method results in imprecision and sometimes in inaccuracies up to 10
303 μT.

304

305 4.2 Validity of the Mean(XYZ) anisotropy correction

306 To further test the reliability of this correction, we performed the Mean(XYZ) and the TRM
307 tensor methods on five samples. The first two, 11369B-1 and 11369B-11, are small bricks
308 baked in an experimental kiln in Sallèles-d'Aude (southern France). The last three, SAQ48,
309 SAQ51 and SAQ54 are pottery sherds discovered in a sedimentary core from Saqqara (Egypt)
310 and supposed to be from the Pharaonic era. Samples were cut in six identical cubic
311 specimens, each positioned in a different position (+x, -x, +y, -y, +z or –z) in the laboratory
312 furnace during the classical Thellier-Thellier protocol and the cooling rate correction. The
313 tensor of TRM anisotropy was then determined with the same protocol as for Chalcatzingo
314 samples. All specimens provided technically reliable intensity results (Figure 1S and Table 3S
315 in Supplementary Material). The degrees of TRM anisotropy have close values between 1.19
316 and 1.26 (Table 2).

317 Table 2 compares the averages intensities of the Mean(XYZ) and TRM anisotropy tensor
318 methods, both being corrected for cooling rate effect. Without the TRM tensor correction, the
319 palaeointensity values at the sample level are distributed over a large range up to 26 μT with
320 systematic differences between axes. The highest palaeointensities values, i.e. the lowest
321 acquired TRMs, are observed for specimens with the laboratory field applied along x axis,
322 perpendicularly to the flattening plane of the brick or the pottery (Veitch et al., 1984). The
323 correction by the TRM tensor groups the palaeointensities, which results in a standard
324 deviation up to five times lower. The Mean(XYZ) average palaeointensity differ of the TRM
325 tensor value by only -5.6 to 3.8% (IE parameter in Table 2). No relationship seems exist
326 between IE and the anisotropy degree or the standard deviation.

327 The anisotropy correction depends on the NRM direction within the TRM tensor. In our
328 examples, the Mean(XYZ) palaeointensity is close to the TRM tensor value, because the

329 NRM direction is intermediate between x, y and z axes and because averages are computed
330 from six specimens with an equal contribution of the three axes. Data with two, and of course
331 one, specimens cannot be considered as corrected by the anisotropy.

332

	Mean(XYZ)					TRM tensor						
Sample	F_{min} (μT)	F_{max} (μT)	F_{mean} (μT)	SD (μT)	SD (%)	F_{min} (μT)	F_{max} (μT)	F_{mean} (μT)	SD (μT)	SD (%)	IE (%)	k_{max}/k_{min}
11369B1	45.0	52.3	50.0	2.6	5.2	51.1	54.4	50.9	1.2	2.3	-1.7	1.19
11369B11	45.0	56.6	47.6	4.4	9.2	49.9	53.4	50.5	1.2	2.3	-5.6	1.25
SAQ48	65.8	79.4	71.5	4.7	6.6	76.0	82.7	74.3	2.5	3.4	-3.7	1.20
SAQ51	74.8	100.7	85.5	11.5	13.5	83.2	87.5	82.3	2.5	3.0	3.8	1.25
SAQ54	74.9	99.3	83.8	9.6	11.5	81.1	89.6	83.1	3.4	4.1	0.8	1.26

333

334 Table 2: Comparison of intensities determined with the two corrections of anisotropy. For
335 both methods are indicated the minimal and maximal specimen intensity, the mean intensity
336 and its standard deviation in microTeslas and in percentage. All intensities are corrected for
337 the cooling rate effect. IE is the difference in percentage of the Mean(XYZ) intensity with the
338 TRM tensor intensity. k_{max}/k_{min} is the average degree of TRM anisotropy.

339

340 A balance between the three axes does not mean that one can be fully confident in the average
341 palaeointensity value. If the NRM is parallel to one of the three axes, the two specimens with
342 the laboratory field on this axis will give the true palaeointensity and the inaccuracy can be
343 larger. In the case of SAQ51, if the NRM were close to x-axis, the true palaeointensity would
344 have been around 102-103 μT, whereas the average of the six specimens is 85.5±11.5 μT
345 (Tab. 3S, Supplementary Material).

346 For all these reasons, the Mean(X-Y-Z) method enhances noise in a dataset with larger
347 standard deviations and possible high inaccuracies. All Mean(XYZ) palaeointensities can be
348 biased even if the risk is reduced for those calculated with a balanced participation of the
349 three x, y and z axes. Data corrected with the TRM tensor are clearly much more reliable
350 from an experimental point of view.

351

352 4.3 Data selection

353 Estimate a posteriori the quality of a palaeointensity is not straightforward without the raw
354 measurements. Four intensities from Rodriguez-Ceja et al. (2009, 2012) have been defined on
355 a secondary component and clearly have to be removed. Another obvious criterion is the
356 expected internal consistency within a given cooling unit. We classified data in three
357 categories according to the number of specimens and the standard deviation (Figure 5c).
358 Highest quality data (category C1) have at least 3 specimens per cooling unit and a standard
359 deviation (SD) lower than 10%. Those in the second category (C2) have a SD lower than
360 15%. Other data (C3) represent 38% of the full dataset (i.e. 72 data) in similar proportions for
361 volcanic and archaeomagnetic data (Figure 5c). One can note that most extreme values are
362 included in this category.

363

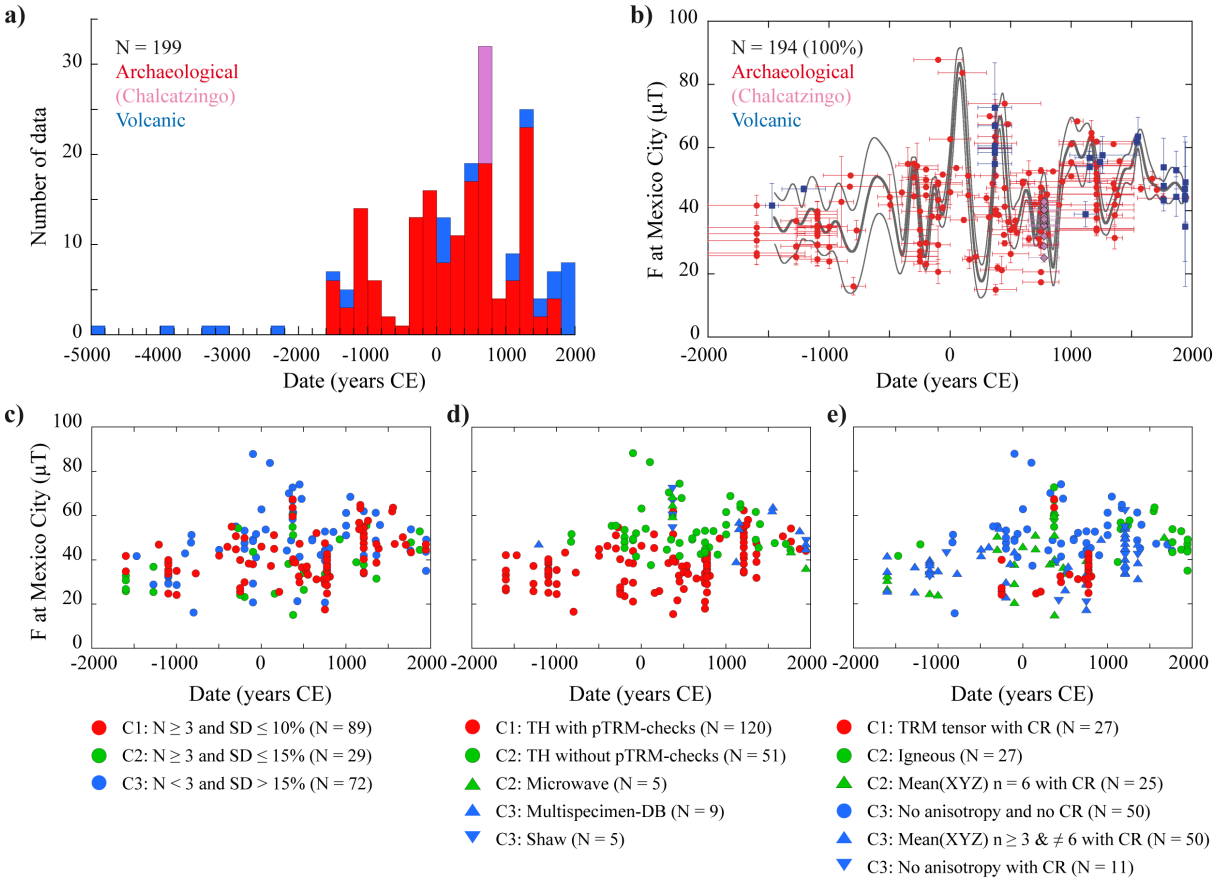

Figure 5: Critical analysis of the Central American palaeointensity dataset. (a) Temporal distribution of data over the last 7 kyrs. (b) Compilation of all archaeomagnetic (in red) and volcanic (in blue) data. The grey curve with its 1σ confidence envelope is computed using a Bayesian method. (c) Ranking of the dataset according to the cooling unit consistency. (d) Ranking according to the quality of the intensity protocol. (e) Ranking according to the consideration of the anisotropy effect. For each criterion, data are ranked in three levels C1, C2 and C3 from the highest to the lowest quality. Plots (c-d-e) excluded four data defined on a secondary component from Rodriguez-Ceja et al. (2009, 2012). TH: Thellier-Thellier protocols; Multispecimen-DB: original multispecimen protocol of Dekkers and Böhnel (2006); N: number of data; For data using Mean(XYZ) anisotropy correction, n: number of specimens used in the average intensity.

377 The criterion of the consistency is useful but cannot screen all problems in the palaeointensity
378 protocol (Figure 5d). For the reasons mentioned above, the most reliable protocol is the
379 Thellier-Thellier protocol with pTRM-checks. This category (C1) is dominant in the dataset
380 (120/190 data). Our mid-quality category (C2) groups microwave data and Thellier-Thellier
381 data without pTRM-checks. We did not assign the latter to the lowest quality category
382 because often it corresponds to the oldest data, as it is the case here (51 data almost all from
383 Bucha et al., 1970 and Lee, 1975), when pTRM-checks were not commonly used.
384 Furthermore, the interpretation of pTRM-checks is not straightforward and experience shows
385 that reliable palaeointensity can be obtained with moderate deviation if the linearity is well
386 maintained over a large NRM proportion. However, the absence of alteration monitoring casts
387 a doubt on the reliability of these data. Finally, the low-quality category (C3) includes the
388 nine multispecimen data without the correction of the NRM fraction (MSP-DB), because they
389 likely overestimate the palaeointensity. The five data acquired with the Shaw protocol also
390 belong to this category.

391

392 As archaeological baked clays constitute 86% of the dataset (164/190 data) whose 85% are
393 ceramics (139 data), cooling rate and anisotropy corrections are crucial. For archaeological
394 baked clays, we demonstrated that the anisotropy correction with the TRM tensor is the most
395 reliable (category C1). Two microwave data on potteries associated to the Xitle lava flow are
396 also included in C1 (Böhnel et al., 2003), because the laboratory field was applied parallel to
397 the NRM. Only 27 data are part of this high-quality category (Figure 5e). Both corrections are
398 assumed not mandatory for igneous material. But this is not fully attested and we preferred to
399 assign these data to the mid-quality C2 category. Regarding the Mean(XYZ) correction, the
400 balanced contribution between x, y, and z axes can be attested only for the 25 average
401 intensities calculated with six specimens. We classified them in the C2 category, bearing in

mind that some can be inaccurate especially if the NRM was parallel to a specimen axis. Another number of specimens gives preponderance to one or two axes, which can result in larger inaccuracies and justifies their attachment to the C3 category. Data calculated with three and four specimens are actually more scattered (Figure 2S, Supplementary Material). The C3 category finally includes the 61 archaeological data without any anisotropy correction, 11 of them being corrected for the cooling rate effect.

The synthesis of this critical analysis ranks the dataset in three groups, C1, C2 and C3. Data of the high quality group (C1) belong to the three C1 categories of the cooling unit consistency, protocol and anisotropy and cooling rate corrections at the same time. They are only 23, i.e. 12% of the initial dataset, (Chalcatzingo data, this study; Fanjat et al., 2013; Rodriguez-Ceja et al., 2009, 2012 – only intensities determined on the characteristic magnetization) , all dated between 400 BCE and 900 CE (Figure 6a).

The group C2 gathers data classified at least in the C2 category for the three criteria. The El Jorullo and Xitle lava flows were duplicated in respectively two and four studies and we computed new averages from the same accepted specimens as the authors (Table 4S, Supplementary Material). In the case of the Xitle, the average (59.8 ± 5.0 μT) takes into account only the palaeointensities corrected for the cooling rate effect on the TRM intensity (Figure 6a).

All other data, those belonging to at least one C3 category, constitute 72% of the dataset (140 data) with almost all the oldest acquired data (Bucha et al., 1970; Lee, 1975). These 50 data on potteries with no anisotropy and cooling rate corrections provide higher palaeointensities than other data (blue circles, Figure 5e). If the weak cooling consistency influences their scatter, the overestimation very likely results from absence of the cooling rate correction.

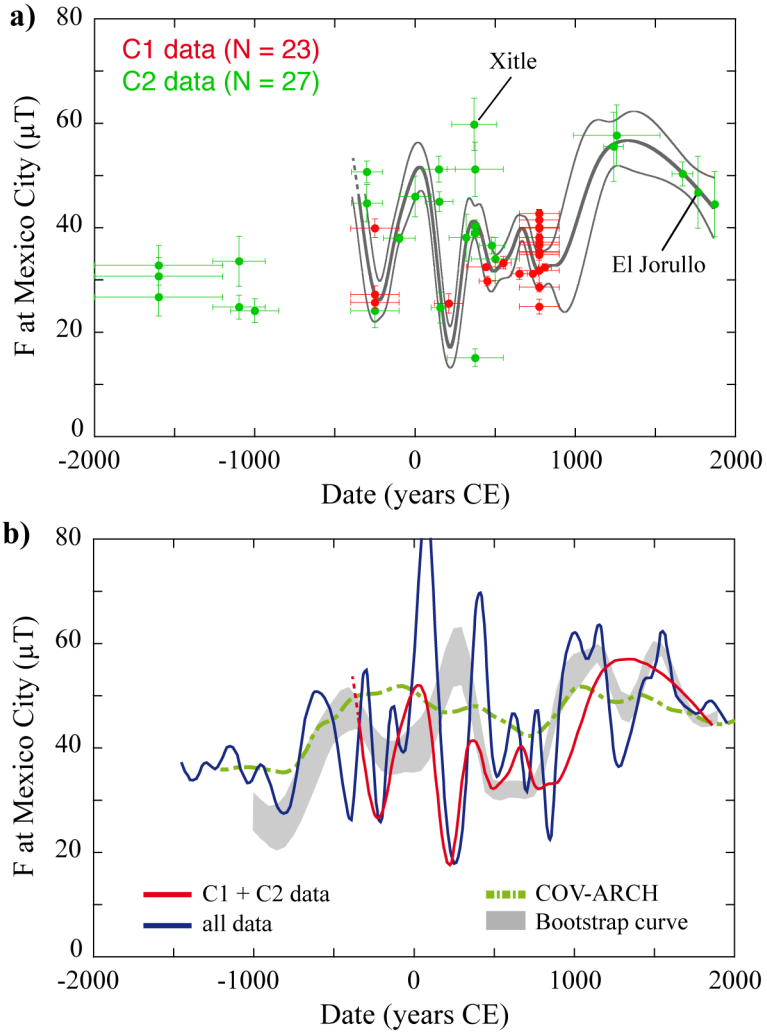

425

426 Figure 6: (a) Secular variation inferred from high-quality data. (b) Comparison of the two
427 Bayesian curves calculated from the total and selected dataset (blue and red curves) with the
428 master curve of Goguitchaichvili et al. (2018a) (grey curve) and with COV-ARCH global
429 model (green dotted curve).

430

431 **6. Discussion**

432 6.1 Impact of the critical analysis on the knowledge of the secular variation

433 The large number of palaeointensities available for the last kyrs in Central America may give
434 the impression that the secular variation curve is well-known, with large and fast variations
435 between 20 and 80 μT. However, the critical analysis shows that many of these oscillations

436 are induced by experimental errors. The main sources of scatter are the absence of cooling
437 unit consistency, the lack or inaccuracy of anisotropy correction and the absence of cooling
438 rate correction on archaeological artefacts. Only 12% of data (23 data) can be considered as
439 high quality (C1 category) that is not enough to compute an intensity secular variation curve.
440 Therefore we also included the 14% of the data (27 data) corresponding to the middle quality
441 (C2 category) (Figure 6a). All data used in the Bayesian curve are plotted per study in Figure
442 3S (Supplementary Material).

443 It is worth pointing out that the selection does not take into account the age uncertainties and
444 inaccuracies in age, perhaps affecting some of the selected data. That could be the case for the
445 Xitle lava flow, whose intensity seems more consistent with an age at the turning point of the
446 Christian era than in the IVth and Vth centuries CE (Figure 6a). We decided to use the most
447 recently acquired age 1670±35 uncal. BP (Siebe, 2000) on a charcoal included in the lava
448 flow sampled for the palaeomagnetic studies. But other published radiocarbon ages, 1945±55
449 uncal BP and 2025±55 uncal BP (Delgado et al., 1998; see also Böhnel et al, 1997), dates the
450 eruption of this monogenetic volcano in a more consistent way with other available quality
451 data.

452 Selecting data has a strong influence on the secular variation reconstruction, as shown by the
453 comparison of the averages Bayesian curves calculated from the entire and selected datasets
454 (blue and red curves, Figure 6b). After discarding extreme values, the secular variation has
455 smaller amplitude between 20 and 60 μT. The better consistency of the dataset also removes
456 most short-term oscillations of the curve calculated with all data.

457 The secular variation from ~400 BCE to ~500 CE is rather well constrained by high/middle
458 quality C1 and C2 data. They highlight a fast variation with a ~45 μT maximum in ~400
459 BCE, a ~25 μT minimum in ~200 BCE, a further ~50 μT maximum circa 0 CE and a ~20 μT

460 minimum in ~200 CE. Next, the field varied more slightly between 30 and 40 μT from ~400
461 to ~800 CE that is the period presenting the highest density of quality data.

462 On the other side, the lack of data and the large age uncertainties make unclear the secular
463 variation between 2000 and 400 BCE. Address this gap is crucial to better understand the
464 highest secular variation and the largest departure from an axial dipolar field observed at this
465 period in Eurasia (Hervé et al., 2017; Shaar et al., 2016).

466 Considering only high or middle quality data drastically reduces the available data set and one
467 may wonder if we do not miss some geomagnetic variations. For example, there are only five
468 high-quality data in the second millennium CE and it is not surprising to see that the curves
469 differ during this period. If the high geomagnetic field strength around 50 μT is well
470 constrained, the number of maxima, one or two, is unclear. Unselected data indicates a
471 possible minimum ~1300 CE. The timing of the intensity increase is also not clear, either
472 from 1000 CE with C1 and C2 categories or from 800 CE with unselected data.

473 Finally, the critical analysis of the Central America dataset drastically highlights the need of
474 new high quality data with precise dating for almost all periods. It is clearly a prerequisite to
475 ascertain the secular variation features and to compare the Central American curve to other
476 regional records.

477

478 6.2 Comparison with others curves and global models

479 Our selected curve presents several differences with the bootstrap curve of Goguitchaichvili et
480 al. (2018a), especially between 500 BCE and 500 CE (Figure 6b). The major discrepancy
481 occurs around 200 CE when they have a maximum and us a minimum. Different reasons
482 could be the source of this inconsistency: i) their critical analysis (at least 4 specimens,
483 standard deviation lower than 10 μT, corrections of anisotropy and cooling rate) is pretty

484 similar to ours except for the inclusion of all Mean(XYZ) data; ii) the dataset of
485 Goguitchaichvili et al. (2018a) duplicated data from the same lava flow (e.g. Xitle, El Jorullo,
486 Ceboruco, Paricutin) and iii) included 17 data from southwest USA but not 28 data from
487 Mexico out of the 50 that we classified in the C1 and C2 categories. Some differences
488 between the curves are also related to the computation technique. The variability of intensity
489 data circa 200 BCE is smoothed by the bootstrap method, whereas the Bayesian of Lanos
490 (2004) interprets it by an intensity minimum. Both updated dataset and Bayesian approach
491 likely provides a finer knowledge of the secular variation curve, even though as mentioned
492 before it has to be confirmed by new reliable data.

493 The global models such as COV-ARCH are built using the Geomagia database without data
494 selection. They are inconsistent with our curve as well as with Goguitchaichvili et al. (2018a)
495 curve (Figure 6b). First, they predict a smoother secular variation after 500 BCE with
496 intensity varying between 40 and 50 μT, this range corresponding to the average intensity of
497 the total dataset. The model did not succeed to interpret the high data variability and remains
498 blocked in this intensity range. Another inconsistency is the shift to higher intensity values in
499 comparison to our curve. The data of Bucha (1970) and Lee (1975), not corrected for the
500 cooling rate, constitute around 40% of the Central American data in Geomagia. The
501 overestimation emphasizes the need for a selection with the cooling rate correction.

502

503 **7. Conclusions**

504 The acquisition of 13 new palaeointensities on Epiclassic (650 – 900 CE) sherds from
505 Chalcatzingo completes the Central American database. The up-to-date compilation of 194
506 available data shows a high variability in palaeointensity during the last 4 millennia. A critical
507 analysis of the database highlights that this variability cannot be only explained by a
508 geomagnetic origin. Selecting data according to the cooling unit consistency and the intensity

509 protocol discards extreme values and predicts less oscillations of the geomagnetic field
510 strength. The results emphasize the importance of the cooling rate correction. Its absence
511 yields to a shift of the geomagnetic reconstructions towards higher intensity values. Another
512 problem, peculiar to the Central American dataset, is the use of an inaccurate anisotropy
513 correction, here called Mean(XYZ). According to experimental test, this method leads to
514 systematic larger imprecisions and to possible inaccuracies up to 15 μT.

515 The example of Central America highlights the need of data selection global geomagnetic
516 model. The absence of data selection clearly plays a role in the smoothing and overestimation
517 of the curves inferred from global models compared to our master curve. Considering these
518 problems, the use of current global models for dating purposes in Central America seems
519 inappropriate.

520 Defining acceptance criteria is not straightforward in global modelling. Our criterion of the
521 cooling unit consistency discards more than 50% of the global dataset and those based on the
522 protocol ~90% (counting on Geomagia50.v3 in October 2018). This low proportion is hardly
523 compatible with the homogeneous data coverage in space and in time that requires the
524 spherical harmonic analysis. Our acceptance limits have to be lowered to better fit with the
525 constraints of global modelling. Priority criteria could focus on parameters biasing the
526 palaeointensity average, such consistency criteria, cooling rate correction for archaeological
527 baked clays and anisotropy correction for potteries.

528

529 **Acknowledgements**

530 Funding was provided by ANR-CONACYT SVPIntMex project ANR-15-CE31-0011-01
531 coordinated by M. P. and L. A-V. G.H. also benefited from a support of Campus France
532 PRESTIGE program (PRESTIGE-2017-1-0002). We thank the editor and the reviewer for

their careful work. We are grateful to Gabrielle Hellio (Univ. Nantes) for transmitting the COV-ARCH and COV-LAKE predictions at Mexico City and to Philippe Lanos for providing the software to calculate Bayesian local secular variation curves. We acknowledge Mohamed Hamdan (Giza University) and Ahmed Saleh (NRIAG) for providing the pottery sherds from Saqqara.

References

Böhnel, H., Morales, J., Caballero Miranda, C., Alva, L., McIntosh, G., Gonzalez, S., & Sherwood, G.J., 1997. Variation of Rock Magnetic Parameters and Plaeointensities over a single Holocne Lava Flow. *J. Geomag. Geoelectr.*, 49, 523-542.

Böhnel, H., Biggin, A., Walton, D. et al., 2003. Microwave palaeointensities from a recent Mexican lava flow, baked sediments and reheated pottery. Earth Planet. Sci. Lett., 214, 221-236, https://doi.org/10.1016/S0012-821X(03)00370-4

Böhnel, H., Pavón-Carrasco, F. J., Sieron, K., & Mahgoub, A. N., 2016. Palaeomagnetic dating of two recent lava flows from Ceboruco volcano, western Mexico. *Geophys. J. Int.*, *207*, 1203–1215. http://doi.org/doi.org/10.1093/gji/ggw310

Brown, M. C., Donadini, F., Korte, M., Nilsson, A., Korhonen, K., Lodge, A., Lengyel, S. N., & Constable, C. G., 2015. GEOMAGIA50.v3: 1. general structure and modifications to the archeological and volcanic database. *Earth Planets Space*, *67*, 1–31. http://doi.org/10.1186/s40623-015-0232-0

Bucha, V., Taylor, R.E., Berger, R., & Haury, E.W., 1970. Geomagnetic intensity changes during the past 3000 years in the western hemisphere. *Science*, 168, 111-114.

Cai, S., Jin, G., Tauxe, L., Deng, C., Qin, H., Pan, Y., & Zhu, R., 2016. Archaeointensity results spanning the past 6 kiloyears from eastern China and implications for extreme behaviors of the geomagnetic field. *Proc. Natl. Acad. Sci. USA*, 114, 39-44.

558 http://doi.org/10.1073/pnas.1616976114
559 Chauvin, A., Garcia, Y., Lanos, P., & Laubenheimer, F., 2000. Paleointensity of the
560 geomagnetic field recovered on archaeomagnetic sites from France. *Phys. Earth Planet.*
561 *Inter.*, *120*, 111–136.
562 Cifuentes-Nava, G., Goguitchaichvili, A., López-Loera, H., Cervantes, M., Cortés, A.,
563 Sánchez-Bettucci, L., Macias, J. L., Morales, J., & Rosas-Elguera, J., 2017. Full vector
564 magnetic dating of some pyroclastic rocks associated to the Colima volcano, western
565 Mexico. *Bol. Soc. Geol. Mex.*, *69*(3), 577–590.
566 Constable, C., Korte, M., & Panovska, S., 2016. Persistent high paleosecular variation activity
567 in southern hemisphere for at least 10 000 years. *Earth Planet. Sci. Lett.*, *453*, 78–86.
568 http://doi.org/10.1016/j.epsl.2016.08.015
569 Dekkers, M. J., & Böhnel, H. N., 2006. Reliable absolute palaeointensities independent of
570 magnetic domain state. *Earth Planet. Sci. Lett.*, *248*, 508–517.
571 http://doi.org/10.1016/j.epsl.2006.05.040
572 Delgado, H., Molinero, R., Cervantes, P., Nieto-Obregon, J., Lozano-Santa Cruz, R., Macias-
573 Gonzalez, H.L., Mendoza-Rosales, C., & Silva-Romo, G., 1998. Geology of Xitle
574 volcano in southern Mexico City – a 2000-year-old monogenetic volcano in an urban
575 area. *Rev. Mex. Cien. Geol.*, 15, 2, 115-131
576 Dodson, M.H., & McClelland-Brown, E., 1980. Magnetic blocking temperatures of single-
577 domain grains during slow-cooling. *J. Geophys. Res.*, 85, 2625-2637.
578 Dunlop, D. J., 2011. Physical Basis of the Thellier-Thellier and Related Paleointensity
579 Methods. *Phys. Earth Planet. Inter.*, *187*(3-4), 118–138.
580 http://doi.org/10.1016/j.pepi.2011.03.006
581 Fabian, K., & Leonhardt, R., 2010. Multiple-specimen absolute palaeointensity
582 determination: an optimal protocol including pTRM normalization, domain-state

583 correction, and alteration test. *Earth Planet. Sci. Lett.*, 297, 84-94.
584 Fanjat, G., Camps, P., Shcherbakov, V., Barou, F., Sougrati, M.T., & Perrin, M., 2012.
585 Magnetic interactions at the origin of abnormal magnetic fabrics in lava flows: a case
586 study from Kerguelen flood basalts. *Geophys. J. Int., 189*, 815-832. doi:10.1111/j.1365-
587 246X.2012.05421.x
588 Fanjat, G., Camps, P., Alva Valdivia, L. M., Sougrati, M. T., Cuevas-Garcia, M., & Perrin,
589 M., 2013. First archeointensity determinations on Maya incense burners from Palenque
590 temples, Mexico: New data to constrain the Mesoamerica secular variation curve. *Earth*
591 *Planet. Sci. Lett.*, *363*, 168–180. http://doi.org/10.1016/j.epsl.2012.12.035
592 Genevey, A., Gallet, Y., Jesset, S., Thébault, E., Bouillon, J., Lefèvre, A., & Le Goff, M.,
593 2016. New archeointensity data from French Early Medieval pottery production (6th–
594 10th century AD). Tracing 1500 years of geomagnetic field intensity variations in
595 Western Europe. *Phys. Earth Planet. Inter.*, *257*, 205–219.
596 http://doi.org/10.1016/j.pepi.2016.06.001
597 Goguitchaichvili, A., Morales, J., Aguayo Haro, R., Quiroz Castañon, H., & Robles Camacho,
598 J., 2016. First evidence of complex dental practice about 1300 BP in Mesoamerica
599 revealed by absolute geomagnetic intensity. *Studia Geophys. Geod.*, *61*.
600 http://doi.org/10.1007/s11200-016-0851-3
601 Goguitchaichvili, A., Ortega, V., Archer, J., Morales, J., & Teran, A., 2017. Absolute
602 geomagnetic intensity record from pre-Columbian pottery dates elite Tlailotlacan
603 Woman in ancient Teotihuacan. *J. Arch. Sci.: Rep.*, *14*, 146–151.
604 http://doi.org/10.1016/j.jasrep.2017.05.030
605 Goguitchaichvili, A., García, R., Pavón-Carrasco, F. J., Morales Contreras, J.J., Soler
606 Arechalde, A.M., & Urrutia-Fucugauchi, J., 2018a. Last three millennia Earth's
607 Magnetic field strength in Mesoamerica and southern United States: Implications in

geomagnetism and archaeology. *Phys. Earth Planet. Inter.*, *279*, 79–91. http://doi.org/10.1016/j.pepi.2018.04.003

Goguitchaitchvili, A., García-Ruiz, R., Echeverría, S., Morales, J., Ortiz, S., & Urrutia-Fucugauchi, J., 2018b. Last two millenia Earth's Magnetic Field strength: New archaeointensity determinations from Ichkaantijo, Early to Late Maya Classic period. *J. Arch. Sci.: Rep.*, *18*, 292–299. http://doi.org/10.1016/j.jasrep.2018.01.023

Goguitchaichvili, A., Cervantes Solano, M., Lazcano Arce, J.C., Serra Puche, M.C., Morales, J., Soler, A.M., & Urrutia-Fucugauchi, J., 2018c. Archaeomagnetic evidence of pre-Hispanic origin of Mezcal. *J. Arch. Sci.: Rep., 21*, 504-511. https://doi.org/10.1016/j/jasrep.2018.08.022

Gómez-Paccard, M., Chauvin, A., Lanos, P., Thiriot, J., & Jiménez-Castillo, P., 2006. Archeomagnetic study of seven contemporaneous kilns from Murcia (Spain). *Phys. Earth Planet. Inter.*, *157*(1-2), 16–32. http://doi.org/10.1016/j.pepi.2006.03.001

Gómez-Paccard, M., Osete, M. L., Chauvin, A., Pavón-Carrasco, F. J., Pérez-Asensio, M., Jiménez, P., & Lanos, P., 2016. New constraints on the most significant paleointensity change in Western Europe over the last two millennia . A non-dipolar origin ? *Earth Planet. Sci. Lett.*, *454*, 55–64. http://doi.org/10.1016/j.epsl.2016.08.024

Grove, D. C., 1987. *Ancient Chalcatzingo*. Austin University Press.

Hellio, G. & Gillet, N., 2018. Time-correlation based regression of the geomagnetic field from archeological and sediment record. *Geophys. J. Int.*, https://doi.org/10.1093/gji/ggy214

Herrero-Bervera, E., 2015. Spot Reading of the Absolute Paleointensity of the Geomagnetic Field Obtained from Potsherds (Age Ca. 500-430 AD) in Teotihuacan, Mexico. *Arch. Disc.*, *3*, 72–84.

Hervé, G., & Lanos, P., 2018. Improvements in archaeomagnetic dating in Western Europe

633 from the Late Bronze to the Late Iron ages: an alternative to the problem of the
634 Hallstattian radiocarbon plateau. *Archaeometry*, 60, 4, 870-883, doi:10.1011/arcm.12344
635 Hervé, G., Chauvin, A., & Lanos, P., 2013. Geomagnetic field variations in Western Europe
636 from 1500 BC to 200 AD. Part II: New intensity secular variation curve. *Phys. Earth*
637 *Planet. Inter.*, *218*, 51–65. http://doi.org/10.1016/j.pepi.2013.02.003
638 Hervé, G., Fassbinder, J., Gilder, S. A., Metzner-Nebelsick, C., Gallet, Y., Genevey, A.,
639 Schnepp, E., Geisweid, L., Pütz, A., Reuss, S., Wittenborn, F., Flontas, A., Linke, R.,
640 Riedel, G., Walter, F., & Westhausen, I., 2017. Fast geomagnetic field intensity
641 variations between 1400 and 400 BCE : New archaeointensity data from Germany. *Phys.*
642 *Earth Planet. Inter.*, *270*, 143–156. http://doi.org/10.1016/j.pepi.2017.07.002
643 Hervé, G., Chauvin, A., Lanos, P., Rochette, P., Perrin, M., & Perron d'Arc, M., accepted.
644 Cooling rate effect on thermoremanent magnetization in archaeological baked clays: an
645 experimental study on modern bricks. *Geophys. J. Int.*
646 Lanos, P., 2004. Bayesian inference of calibration curves: application to archaeomagnetism.
647 In C. E. Buck & A. R. Millard (Eds.), *Tools for constructing chronologies: Crossing*
648 *disciplinary boundaries* (Lecture No, pp. 43–82). London: Springer.
649 Lee, S., 1975. *Secular variation of the intensity of the geomagnetic field during the past 3,000*
650 *years in North, Central and South America*. University of Oklahoma.
651 Licht, A., Hulot, G., Gallet, Y., & Thébault, E., 2013. Ensembles of low degree
652 archeomagnetic field models for the past three millennia. *Phys. Earth Planet. Inter.*, *224*,
653 38–67. http://doi.org/10.1016/j.pepi.2013.08.007
654 Lifton, N., 2016. Implications of two Holocene time-dependent geomagnetic models for
655 cosmogenic nuclide production rate scaling. *Earth Planet. Sci. Lett.*, *433*, 257–268.
656 http://doi.org/10.1016/j.epsl.2015.11.006
657 Lopez-Sanchez, J., McIntosh, G., Osete, M. L., del Campo, A., Villalaín, J. J., Perez, L.,

Kovacheva, M., & Rodriguez de la Fuente, O., 2017. Epsilon iron oxide: origin of the high coercivity stable low Curie temperature magnetic phase found in heated archeological materials. *Geochem. Geophys. Geosyst.*, *18*(7), 2646–2656. http://doi.org/10.1002/2017GC006929

Lopez-Tellez, J. M., Aguilar-Reyes, B., Morales, J., Goguitchaichvili, A., Calvo-Rathert, M., & Urrutia-Fucugauchi, J., 2008. Magnetic characteristics and archeointensity determination on Mesoamerican Pre-Columbian Pottery from Quiahuiztlan, Veracruz, Mexico. *Geof. Int.*, *47*(4), 329–340.

Mahgoub, A. N., Reyes-Guzmán, N., Böhnel, H., Siebe, C., Pereira, G., & Dorison, A., 2017a. Paleomagnetic constraints on the ages of the Holocene Malpaís de Zacapu lava flow eruptions , Michoacán (México): Implications for archeology and volcanic hazards. *The Holocene*. http://doi.org/10.1177/0959683617721323

Mahgoub, A.N., Böhnel, H., Siebe, C., & Chevrel, M., 2017b. Paleomagnetic study of El Metate shield volcano (Michoacán, Mexico) confirms its monogenetic nature and young age (~ 1250 CE). *J. Volc. Geoth. Res.*, *336*, 209–218. http://doi.org/10.1016/j.jvolgeores.2017.02.024

Martin Arana, R., 1987. Classic and Postclassic Chalcatzingo. In Grove, D.C., *Ancient Chalcatzingo*, University of Texas Press, Austin, 387-399.

Michalk, D. M., Biggin, A. J., Knudsen, M. F., Böhnel, H. N., Nowaczyk, N. R., Ownby, S., & López-Martínez, M., 2010. Application of the multispecimen palaeointensity method to Pleistocene lava flows from the Trans-Mexican Volcanic Belt. *Phys. Earth Planet. Inter.*, *179*, 139–156. http://doi.org/10.1016/j.pepi.2010.01.005

Molina Cardin, A., Campuzano, S.A., Osete, M.L., Rivero-Montero, M., Pavon-Carasco, F.J., Palencia-Ortas, A., et al., 2018. Updated Iberian archaeomagnetic catalogue: new full vector paleosecular variation curve for the last 3 millennia. *Geochem. Geophys.*

683 *Geosyst.*, *19* (10), 3637-3656.
684 Morales, J., Alva-Valdivia, L., Goguitchaichvili, A., et al., 2006. Cooling rate corrected
685 paleointensities from the Xitle lava flow: Evaluation of within-site scatter for single
686 spot-reading cooling units. Earth Planets Space, 58, 1341-1347,
687 https://doi.org/10.1186/BF03352630
688 Morales, J., Goguitchaichvili, A., Aguilar-Reyes, B. A., Pineda, M., Carvallo, C., Beramendi-
689 Orosco, L., Gonzalez Hernadez, G., & Oliveros, A., 2012. Rock-Magnetic and
690 Archaeointensity Investigation of Pottery and a Burned Floor at the Tzintzuntzan
691 Archaeological Site, Western Mexico. *Geoarch.*, *27*, 521–537.
692 http://doi.org/10.1002/gea.21426
693 Morales, J., Goguitchaichvili, A., Ángeles Olay Barrientos, M., Carvallo, C., & Aguilar
694 Reyes, B., 2013. Archeointensity investigation on pottery vestiges from Puertas de
695 Rolón, Capacha culture: In search for affinity with other Mesoamerican pre-Hispanic
696 cultures. *Studia Geophys. Geod.*, *57*(4), 605–626. http://doi.org/10.1007/s11200-012-
697 0878-z
698 Morales, J., Fernández, G., Gogichaisvilli, A., Cárdenas, E., Sol, M., & Bernal, H., 2015.
699 Archeomagnetic dating of some Pre-Columbian pottery fragments from northern
700 Mesoamerica : Implications for the chronology of central Mexico during the Epiclassic
701 period. *J. Arch. Sci.: Rep.*, *4*, 32–43. http://doi.org/10.1016/j.jasrep.2015.08.027
702 Nilsson, A., Holme, R., Korte, M., Suttie, N., & Hill, M., 2014. Reconstructing Holocene
703 geomagnetic field variation: New methods, models and implications. *Geophys. J. Int.*,
704 *198*(1), 229–248. http://doi.org/10.1093/gji/ggu120
705 Osete, M.-L., Chauvin, A., Catanzariti, G., Jimeno, A., Campuzano, S. A., Benito-Batanero, J.
706 P., Tabernero-Galan, C., Roperch, P. (2016). New archaeomagnetic data recovered from
707 the study of celtiberic remains from central Spain (Numantia and Ciadueña , 3rd-1st

centuries BC). Implications on the fidelity of the Iberian paleointensity database. *Phys. Earth Planet. Inter.*, *260*, 74–86. http://doi.org/10.1016/j.pepi.2016.09.006

Palencia-Ortas, A., Osete, M. L., Campuzano, S. A., McIntosh, G., Larrazabal, J., & Sastre, J., 2017. New archaeomagnetic directions from Portugal and evolution of the geomagnetic field in Iberia from Late Bronze Age to Roman Times. *Phys. Earth Planet. Inter.*, *270*, 183–194. http://doi.org/10.1016/j.pepi.2017.07.004

Panovska, S., Korte, M., Finlay, C. C., & Constable, C. G., 2015. Limitations in paleomagnetic data and modelling techniques and their impact on Holocene geomagnetic field models. *Geophys. J. Int.*, *202*, 402–418. http://doi.org/10.1093/gji/ggv137

Pavón-Carrasco, F. J., Osete, M. L., Torta, J. M., & De Santis, A., 2014a. A geomagnetic field model for the Holocene based on archaeomagnetic and lava flow data. *Earth Planet. Sci. Lett.*, *388*, 98–109. http://doi.org/10.1016/j.epsl.2013.11.046

Pavón-Carrasco, F. J., Gomez-Paccard, M., Hervé, G., Osete, M. L., & Chauvin, A., 2014b. Intensity of the geomagnetic field in Europe for the last 3 ka: Influence of data quality on geomagnetic field modeling. *Geochem. Geophys. Geosyst.*, 1–16. http://doi.org/10.1002/2014GC005311

Poletti, W., Trindade, R. I. F., Hartmann, G. A., Damiani, N., & Rech, R. M., 2016. Archeomagnetism of Jesuit Missions in South Brazil (1657 – 1706 AD) and assessment of the South American database. *Earth Planet. Sci. Lett.*, *445*, 36–47. http://doi.org/10.1016/j.epsl.2016.04.006

Reimer, P. J., Bard, E., Bayliss, A., Beck, J. W., Blackwell, P. G., Bronk, C., … Edwards, R. L., 2013. INTCAL13 and MARINE13 radiocarbon age calibration curves 0-50,000 years Cal BP. *Radiocarbon*, *55*(4), 1869–1887.

Rodriguez-Ceja, M., Goguitchaichvili, A., Morales, J., Ostrooumov, M., Manzanilla, L. R., Reyes, B. A., & Urrutia-Fucugauchi, J., 2009. Integrated archeomagnetic and micro –

733 Raman spectroscopy study of pre-Columbian ceramics from the Mesoamerican
734 formative village of Cuanalan, Teotihuacan Valley, Mexico. *J. Geophys. Res.*,
735 *114*(B04103). http://doi.org/10.1029/2008JB006106
736 Rodriguez-Ceja, M., Soler-Arechalde, A. M., Morales, J., & Goguitchaishvili, A., 2012.
737 Estudios de arqueointensidad y propiedades magneticas de ceramicas teotihacanas. Una
738 aportacion a la cronologia de Mesoamerica. *In* Manzanilla, L.R. (Ed.), *Estudios*
739 *arqueométricos del centro de barrio de Teopancazco en Teotihuacan*. Mexico City:
740 CICCH UNAM.
741 Schnepp, E., Obenaus, M., & Lanos, P., 2015. Posterior archaeomagnetic dating: An example
742 from the Early Medieval site Thunau am Kamp, Austria. *J. Arch. Sci: Rep.*, *2*, 688–698.
743 http://doi.org/10.1016/j.jasrep.2014.12.002
744 Schnepp, E., Leonhardt, R., Korte, M., & Klett-Drechsel, J., 2016. Validity of
745 archaeomagnetic field recording : An experimental pottery kiln at Coppengrave,
746 Germany. *Geophys. J. Int., 205*, 622–635.
747 Shaar, R., Ben-Yosef, E., Ron, H., Tauxe, L., Agnon, A., & Kessel, R., 2011. Geomagnetic
748 field intensity: How high can it get? How fast can it change? Constraints from Iron Age
749 copper slag. *Earth Planet. Sci. Lett.*, *301*(1-2), 297–306.
750 http://doi.org/10.1016/j.epsl.2010.11.013
751 Shaw, J., 1974. A new method of determining the magnitude of the palaeomagnetic field:
752 Application to five historic lavas and five archaeological samples. *Geophys. J. R. Astron.*
753 *Soc., 39*, 133-141.
754 Siebe, C., 2000. Age and archaeological implications of Xitle volcano , southwestern Basin of
755 Mexico-City. *Journal of Volcanology and Geothermal Research*, *104*, 45–64.
756 Tema, E., Herrero-Bervera, E., & Lanos, P., 2017. Geomagnetic field secular variation in
757 Pacific Ocean : A Bayesian reference curve based on Holocene Hawaiian lava flows.

Earth Planet. Sci. Lett., *478*, 58–65. http://doi.org/10.1016/j.epsl.2017.08.023

Terán-Gerrero, A., Goguitchaichvili, A., Esparza, R., Morales, J., Rosas, J., Soler-Arechalde, A. M., Cardenas, E., & Urrutia-Fucugauchi, J., 2016. A detailed rock-magnetic and archaeomagnetic investigation on wattle and daub building (Bajareque) remains from Teuchitlán tradition (nw Mesoamerica). *J. Arch. Sci.: Rep*, *5*, 564–573. http://doi.org/10.1016/j.jasrep.2016.01.010

Thellier, E., & Thellier, O., 1959. Sur l'intensité du champ magnétique terrestre dans le passé historique et géologique. *Ann. Géophys.*, *15*, 285–376.

Veitch, R. J., Hedley, I. G., & Wagner, J. J. (1984). An investigation of the intensity of the geomagnetic field during Roman times using magnetically anisotropic bricks and tiles. In *Archaeological Sciences* (pp. 359–373). Geneva.

Walton, D., 1991. A new technique for determining palaeomagnetic intensities. *J. Geomag. Geoelec.*, *43*, 333–339.

Walton, D., & Böhnel, H. N., 2008. The microwave frequency method. *Phys. Earth Planet. Inter.*, *167*, 145–148. http://doi.org/10.1016/j.pepi.2008.02.012

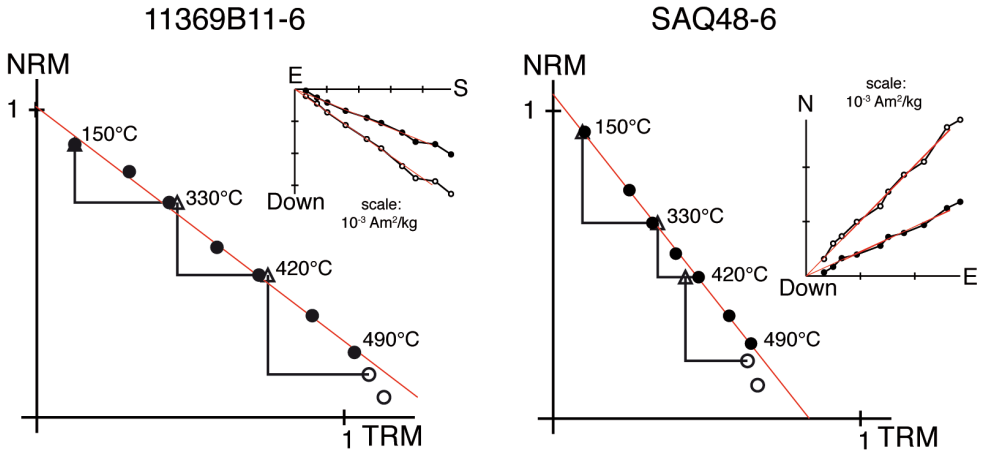

Figure 1S: Representative archaeointensity results of specimens used to test the two anisotropy protocols. The laboratory field was fixed to 60 µT. The specimen on the left is a brick from Sallèles-d'Aude and the one on the right a pottery sherd from Saqqara.

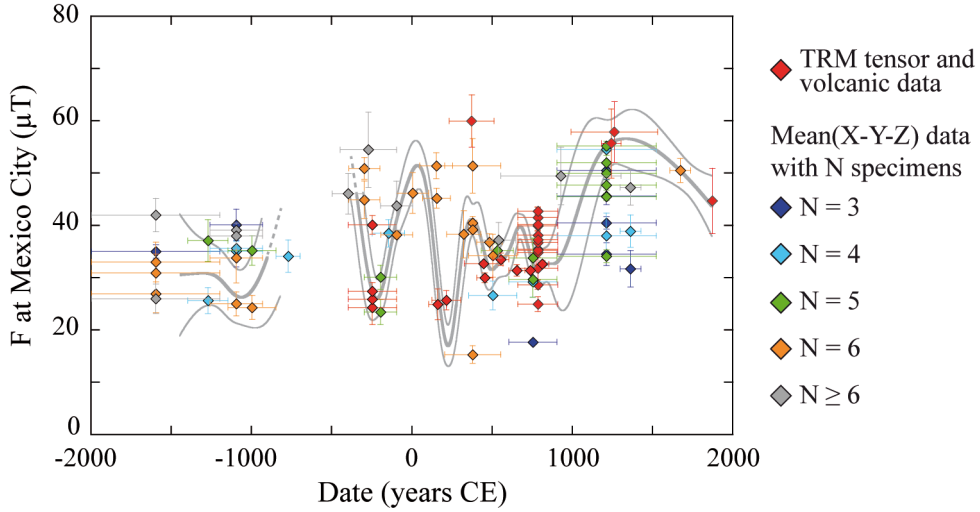

Figure 2S: Influence of the number of specimens on the Mean(X-Y-Z) palaeointensities. Data with highest quality protocol are plotted in red. The Bayesian curve, the same as in Figure 6a, is calculated from C1 and C2 data.

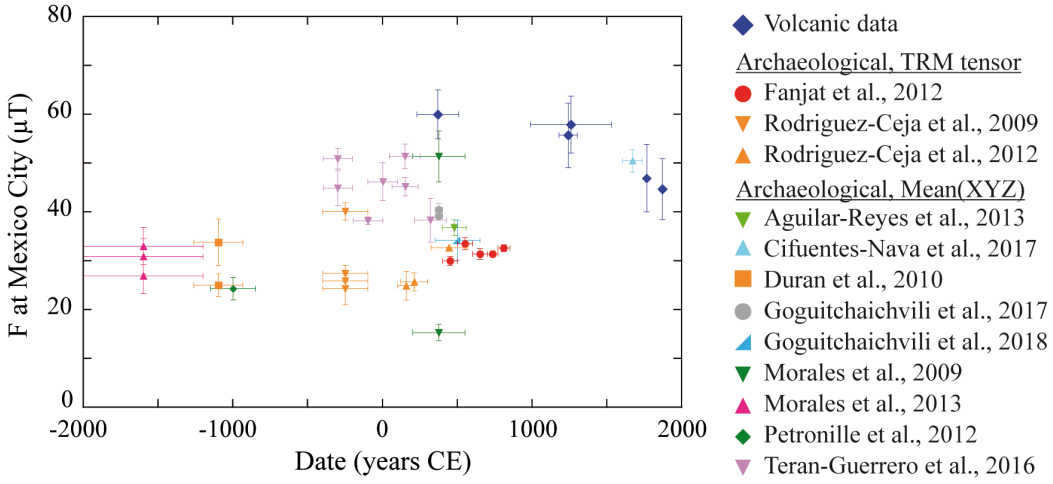

Figure 3S: Highest quality data (C1 and C2 categories) per study. Data from Chalcatzingo (this study) are not plotted here.